Blind Image Deblurring with Outlier Handling

Jiangxin Dong[1] Jinshan Pan[2] Zhixun Su[1,4] Ming-Hsuan Yang[3]
[1]Dalian University of Technology [2]Nanjing University of Science and Technology [3]UC Merced
[4]Guilin University of Electronic Technology
dongjxjx@gmail.com sdluran@gmail.com zxsu@dlut.edu.cn mhyang@ucmerced.edu

Abstract

Deblurring images with outliers has attracted considerable attention recently. However, existing algorithms usually involve complex operations which increase the difficulty of blur kernel estimation. In this paper, we propose a simple yet effective blind image deblurring algorithm to handle blurred images with outliers. The proposed method is motivated by the observation that outliers in the blurred images significantly affect the goodness-of-fit in function approximation. Therefore, we propose an algorithm to model the data fidelity term so that the outliers have little effect on kernel estimation. The proposed algorithm does not require any heuristic outlier detection step, which is critical to the state-of-the-art blind deblurring methods for images with outliers. We analyze the relationship between the proposed algorithm and other blind deblurring methods with outlier handling and show how to estimate intermediate latent images for blur kernel estimation principally. We show that the proposed method can be applied to generic image deblurring as well as non-uniform deblurring. Experimental results demonstrate that the proposed algorithm performs favorably against the state-of-the-art blind image deblurring methods on both synthetic and real-world images.

1. Introduction

Single image deblurring has received considerable attention in recent years as more photos are taken using handheld devices, especially with mobile smartphones. Although most existing smartphones are equipped with anti-shake features, inevitable camera shake results in blurred images when taking photos in low-light conditions. Numerous deblurring algorithms [1, 3, 5, 10, 11, 12, 13, 14, 16, 21, 23, 24, 25, 33] have been developed to address motion blur. The success of these methods can be mainly attributed to the use of statistical priors from natural images (*e.g.*, heavy-tailed distribution of image gradients [5, 25], normalized sparsity prior [13], L_0-regularized priors [20, 32, 33], internal patch recurrence [19], and dark channel prior [23]) and salient edge selection for kernel estimation [3, 31]. Although most existing methods are able to address blurred images with a small amount of noise, these approaches are not effective in handling blurred images with significant outliers, such as saturated pixels and non-Gaussian noise.

Handling blurred images with significant outliers is challenging, and existing methods [4, 29] mainly address the effects of outliers for non-blind deblurring. To address blurred images with outliers in blind image deblurring, one type of methods depends heavily on domain-specific properties, *e.g.*, light streaks [8, 18]. These methods are less effective when the light streaks cannot be extracted and do not perform well for other types of outliers, *e.g.*, non-Gaussian noise. Recently, Pan *et al*. [22] propose an outlier handling method to improve the blur kernel estimation. This method first selects salient edges and then detects the regions of outliers to refine the edge information for blur kernel estimation. Although this method performs well on several kinds of outliers, *e.g.*, saturated pixels and non-Gaussian noise, it needs complex operations and does not deblur images well when the edges are not correctly selected or the regions of outliers cannot be detected.

It is well known that the outliers significantly affect the goodness-of-fit in function approximation. Thus, when outliers exist, the intermediate latent images estimated by the methods with conventional data fidelity terms [15] contain significant artifacts and blur residues (Figure 2), which accordingly affects the blur kernel estimation process. This is the main reason why most existing blind deblurring approaches are less effective in handling blurred images with outliers. In this paper, we propose a simple yet effective method that is able to minimize the effects of outliers on the blur kernel estimation. In contrast to existing outlier handling algorithms [8, 18, 22], the proposed method does not require complex operations, *e.g.*, light streak detection [8, 18] and outlier detection [22], which are vital for existing outlier handling methods to estimate blur kernels.

The contributions of this work are summarized as follows. First, we propose a robust method to measure the goodness-of-fit so that the effects of outliers can be minimized in the blur kernel estimation process. Second, we

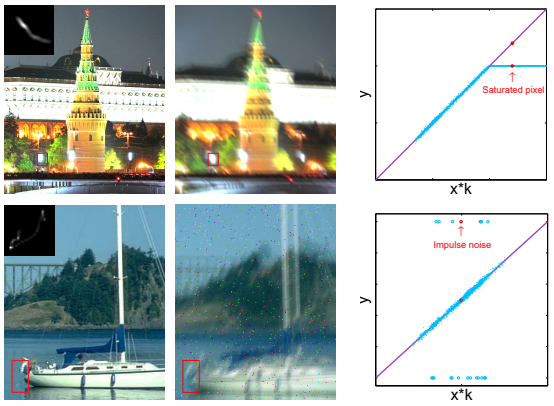

(a) x and k (b) y (c) Relation of y and $x * k$

Figure 1. Properties of saturated pixels and impulse noise. (a) Clear images x with the blur kernels k. (b) Blurred images y with saturated pixels (top) and impulse noise (bottom). (c) Blue points: the relation between y and $x * k$. Purple lines: the ideal case of $y = x * k$.

present the detailed analysis on how the proposed method performs in the blur kernel estimation process from two perspectives, including its mathematical essence and its weight in the iteratively re-weighted least squares (IRLS) [15] optimization. Third, we discuss the relation between the proposed algorithm and other methods concerning outlier handling and show that the proposed method generates reliable intermediate results for blur kernel estimation without ad-hoc detection processes. Furthermore, the proposed method performs favorably against state-of-the-art blind deblurring methods on both synthetic and real-world images with significant outliers. Finally, the proposed algorithm is extended to handle the non-uniform deblurring effectively.

2. Proposed Method

In this section, we develop a robust method within the maximum a posteriori (MAP) framework to handle outliers for blind image deblurring. We first discuss the motivation behind the proposed method and the effects of outliers on data fidelity terms as well as the blur kernel estimation.

2.1. Motivation

A blurred image y can be modeled as a clear image x convolved with a blur kernel k and the noise n:

$$y = x * k + n, \tag{1}$$

where $*$ denotes the convolution operator. However, some intensity values of y are quite different from those of $x * k$ due to the effect of outliers, *e.g.*, saturated pixels and impulse noise (Figure 1), which cannot be well modeled by the linear convolution model (1) and will affect both the latent image estimation and the blur kernel estimation.

Most deblurring methods are based on the linear convolution model (1), while the outliers usually have significant effects on the goodness-of-fit (Figure 1). Thus, existing approaches may consider the outliers as the useful information, *e.g.* the salient edge, which will accordingly affect the blur kernel estimation process. We note that although some image priors are able to handle saturated pixels by exploiting intensity information [20, 23], these image priors are derived based on the noise-free images and are less effective for non-Gaussian noise.

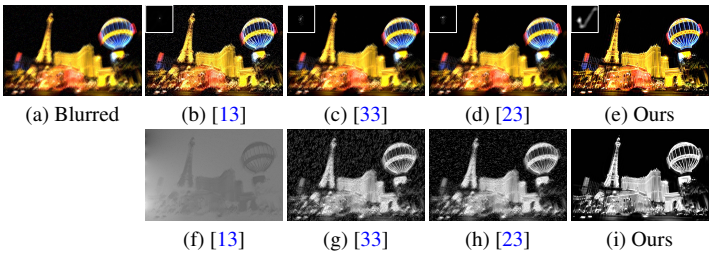

(a) Blurred (b) [13] (c) [33] (d) [23] (e) Ours

(f) [13] (g) [33] (h) [23] (i) Ours

Figure 2. Effects of outliers on blur kernel estimation. (b)-(e) Deblurred images. (f)-(i) Intermediate latent images in the kernel estimation.

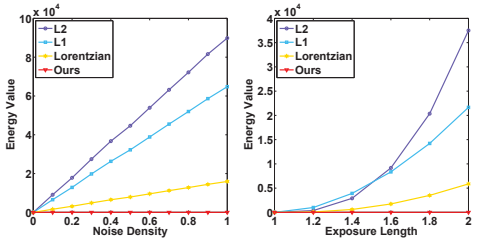

(a) Impulse noise (b) Saturated pixels

Figure 3. Effects of outliers on the metrics used in the conventional data fidelity terms. Each curve shows the goodness-of-fit at different noise level and exposure length. The noise density denotes the proportion of pixels affected by noise in an image. The exposure length denotes the exposure time. The examples of impulse noise and saturated pixels are shown in Figure 1.

Figure 2 shows some deblurred results with corresponding intermediate latent images generated by the methods with different image priors. Due to outliers, state-of-the-art methods are less effective in deblurring these images.

Effect of outliers on data fidelity terms. The commonly used data fidelity term in blind image deblurring is based on ℓ_2-norm. However, the deblurring methods based on this data fidelity term are not robust to outliers as shown in [4, 22]. Although the deblurring methods based on the data fidelity terms with ℓ_1-norm [31] or Lorentzian function [2] are able to handle outliers, *e.g.*, impulse noise, to certain extent, these approaches are less effective when the noise density is higher or the exposure length is longer (more saturated pixels) [4, 22].

Figure 3 shows the effects of outliers, *i.e.*, impulse noise and saturated pixels, on the data fidelity terms. In Figure 3, the values of the data fidelity terms based on ℓ_2-norm, ℓ_1-norm, and Lorentzian function significantly increase as the noise density or exposure length increases, which indicate that outliers dramatically affects the goodness-of-fit and these data fidelity terms are sensitive to outliers. Therefore, deblurring methods based on these data fidelity terms are less effective for images with outliers.

Recent outlier handling methods. In [8], Hu *et al*. develop a light streak detection method and use the light streak information to guide kernel estimation. Pan *et al*. [22] detect the positions of outliers and remove them from salient edges for kernel estimation. We note existing methods operate on the same premise of detecting and removing outliers to minimize the adversarial effects on kernel estimation process. In essence, existing outlier handling processes used in [8, 22] aim to make the goodness-of-fit of the data fidelity term more reliable. This is the main reason that recent outlier handling methods [8, 22] is able to handle blurred images with outliers.

As explained above, the data fidelity term plays a critical role in image deblurring with outliers. Although this problem has been extensively studied in machine learning problem, it receives much less attention in image deblurring as the outliers may result from non-Gaussian noise and saturated pixels. According to the robust analysis [9], a good data fidelity term should satisfy that its value is not sensitive to the large error (Figure 1). Based on this criterion, we adopt a new data fidelity term in the kernel estimation based on a robust function, which is defined as

$$\mathcal{R}(z) = \frac{z^2}{2} - \frac{\log(a + e^{bz^2})}{2b}, \tag{2}$$

where a and b are positive scalar parameters. This function is robust to outliers as shown in Figure 3. More detailed analysis on (2) in blind image deblurring is provided in Section 4.1.

2.2. Proposed Model

Based on above analysis, we estimate the latent image x and the blur kernel k from the blurred image y based on the MAP framework. The proposed deblurring model is

$$\min_{x,k} \mathcal{R}(x * k - y) + \gamma \mathcal{P}_k(k) + \lambda \mathcal{P}_x(x), \tag{3}$$

where $\mathcal{P}_k(k)$ and $\mathcal{P}_x(x)$ are priors on the blur kernel k and the latent image x; γ and λ are weights to balance these two priors. More analysis about how the proposed algorithm performs on blind image deblurring and its robustness to outliers is discussed in Section 4.1. Note that the data fidelity term is introduced for uniform deblurring first, but can be applied to non-uniform deblurring (see Section 5).

3. Optimization

The deblurring process is modeled as the optimization problem by alternatively solving the latent image x

$$\min_{x} \mathcal{R}(x * k - y) + \lambda \mathcal{P}_x(x), \tag{4}$$

and the blur kernel k,

$$\min_{k} \mathcal{R}(x * k - y) + \gamma \mathcal{P}_k(k). \tag{5}$$

To maintain the sparsity of blur kernels, we use the ℓ_1 norm to regularize the intensity of k [22], i.e., $\mathcal{P}_k(k) = \|k\|_1$. For the image prior, we use the hyper-Laplacian prior proposed by Levin *et al*. [15] and set $\mathcal{P}_x(x) = \|\nabla x\|_p$, $p = 0.8$ in our model. The optimization details of these two sub-problems are described in the following sections.

3.1. Estimating Latent Image x

With the blur kernel k from the previous iteration, the intermediate latent image x is estimated by

$$\min_{x} \mathcal{R}(x * k - y) + \lambda \|\nabla x\|_{0.8}. \tag{6}$$

It is difficult to solve this optimization problem due to the non-linear function $\mathcal{R}(\cdot)$. We use the IRLS [15] method to solve (6). At each iteration, we need to solve the quadratic problem:

$$\begin{aligned} x^{[t+1]} = \arg\min_{x} \sum_{\mathrm{p}} \{ & \omega^x |(x * k - y)_{\mathrm{p}}|^2 \\ & + \lambda(\omega_h^x |(\partial_h x)_{\mathrm{p}}|^2 + \omega_v^x |(\partial_v x)_{\mathrm{p}}|^2)\}, \end{aligned} \tag{7}$$

where $\omega^x = \frac{\mathcal{R}'((x^{[t]} * k - y)_{\mathrm{p}})}{(x^{[t]} * k - y)_{\mathrm{p}}}$, $\mathcal{R}'(\cdot)$ is the derivative function of $\mathcal{R}(\cdot)$, $\omega_h^x = |(\partial_h x^{[t]})_{\mathrm{p}}|^{-1.2}$, $\omega_v^x = |(\partial_v x^{[t]})_{\mathrm{p}}|^{-1.2}$, t denotes the iteration index, and the subscript p denotes the spatial location of a pixel. We note that (7) is a weighted least squares problem which can be solved by the conjugate gradient method.

3.2. Estimating Blur Kernel k

Given the intermediate latent image x, the blur kernel k can be obtained by solving (5). As the kernel estimation based on image gradients has been shown to be more accurate [3, 25, 33], we replace the image intensity with the image derivatives in the data fidelity term and estimate the blur kernel k by

$$\min_{k} \mathcal{R}(\nabla x * k - \nabla y) + \gamma \|k\|_1. \tag{8}$$

Similar to (6), we use the IRLS method to solve (8) by

$$\begin{aligned} k^{[t+1]} = \arg\min_{k} \sum_{\mathrm{p}} \{ & \omega_h^k |(\partial_h x * k - \partial_h y)_{\mathrm{p}}|^2 \\ & + \omega_v^k |(\partial_v x * k - \partial_v y)_{\mathrm{p}}|^2 + \gamma \omega^k |k_{\mathrm{p}}|^2\}, \end{aligned} \tag{9}$$

where $\omega_h^k = \frac{\mathcal{R}'((\partial_h x * k^{[t]} - \partial_h y)_{\mathrm{p}})}{(\partial_h x * k^{[t]} - \partial_h y)_{\mathrm{p}}}$, $\omega_v^k = \frac{\mathcal{R}'((\partial_v x * k^{[t]} - \partial_v y)_{\mathrm{p}})}{(\partial_v x * k^{[t]} - \partial_v y)_{\mathrm{p}}}$, and $\omega^k = \frac{1}{|k_{\mathrm{p}}^{[t]}|}$. The conjugate gradient method is used to solve (9).

After obtaining k, we set the negative elements to 0, and normalize it so that the sum of its elements is 1. Similar to the state-of-the-art methods, the proposed kernel estimation process is carried out in a coarse-to-fine manner using an image pyramid. In the coarsest level, x and k are initialized as the blurred image and delta kernel, respectively. Algorithm 1 shows the main steps for the kernel estimation algorithm on one pyramid level.

Algorithm 1 Blur kernel estimation algorithm

Input: Blurred image y.
initial k with results from the coarser level.
for $i \leq t_{\max}$ **do**
  Estimate x according to (7).
  Estimate k according to (9).
end for
Output: Blur kernel k and latent image x.

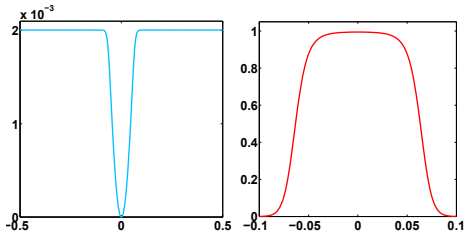

(a) $\mathcal{R}(z)$ (b) $\frac{\mathcal{R}'(z)}{z}$

Figure 4. Visualization of the robust function $\mathcal{R}(z)$ and the weight, *i.e.*, $\frac{\mathcal{R}'(z)}{z}$, used in IRLS.

4. Analysis of Proposed Method

In this section, we analyze how the proposed algorithm performs on blind image deblurring with outliers. We also demonstrate the effectiveness of the proposed data fidelity term for blur kernel estimation with outlier handling. In addition, we discuss the relationship of the proposed algorithm with other methods in terms of handling outliers.

4.1. Effectivness of Proposed Method

As discussed in Section 2.1, the proposed data fidelity term is robust to outliers. From the definition of the robust function (2), the Taylor polynomial approximation of $\mathcal{R}(z)$ with respect to z at 0 is

$$\mathcal{R}(z) = \frac{a}{2a+2}z^2 - \frac{\log(a+1)}{2b} + O(z^3), \qquad (10)$$

where $O(\cdot)$ denotes the equivalent infinitesimal. The Taylor expansion of $\mathcal{R}(z)$ means that $\mathcal{R}(z)$ has the same order with z^2 if the value of z is close to zero. This property demonstrates that the proposed intermediate latent image estimation model (4) will reduce to the sparse deconvolution model by Levin *et al*. [16], which is effective for the image deconvolution without outliers. Figure 4 shows that $\mathcal{R}(z)$ is close to a constant when the value of z is large[1]. In this case, the model (4) reduces to a constant plus the regularization term. Thus, only the regularization term has an effect on the image restoration, which indicates that most outliers will be smoothed. This property ensures that the deblurring method based on (2) is able to handle outliers.

From the perspective of the IRLS iteration, the weight for the data fidelity term is $\frac{\mathcal{R}'(z)}{z}$. It has a small value when a pixel is an outlier; otherwise, it has a large value (Figure 4(b)). This indicates that the outliers have less effect on both the intermediate latent image estimation and blur kernel estimation. Figure 5(m)-(o) show the visualizations of the weights (*i.e.*, ω_h^k, ω_v^k, and ω^x) in blur kernel estimation and the latent image estimation, where the dark pixels in the weight maps indicate the positions of outliers. In addition, we note that $\frac{\mathcal{R}'(z)}{z}$ is similar to the outlier detection function used in [22], which demonstrates the effectiveness of the proposed method.

To further demonstrate the effectiveness of the proposed data fidelity term, we compare it with conventional data fi-

[1]The value of $(x * k - y)$ at pixel p is large if pixel p is an outlier, and is small otherwise (Figure 1).

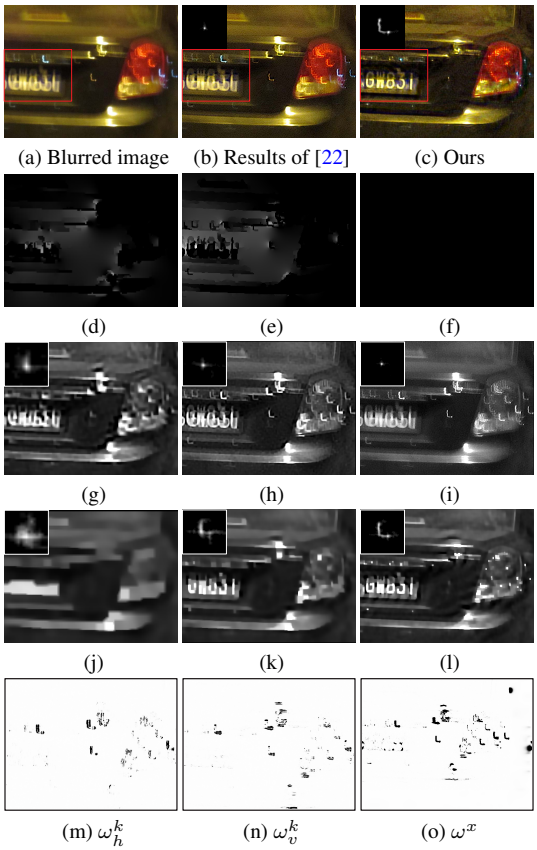

(a) Blurred image (b) Results of [22] (c) Ours
(d) (e) (f)
(g) (h) (i)
(j) (k) (l)
(m) ω_h^k (n) ω_v^k (o) ω^x

Figure 5. Comparison with Pan *et al*. [22]. (d)-(f) Edge selection results during the iterations by [22]. (g)-(i) and (j)-(l) Intermediate latent images with estimated kernels during the iterations by [22] and the proposed method, respectively. (m)-(o) Weight maps (see Section 3.1 and 3.2) of the proposed method in the kernel estimation and the latent image estimation.

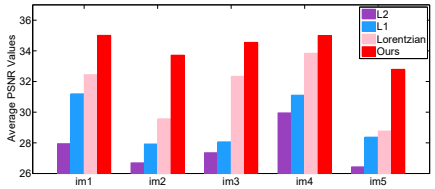

Figure 6. Quantitative evaluation of the proposed data fidelity term and conventional data fidelity terms on the proposed dataset with saturated pixels.

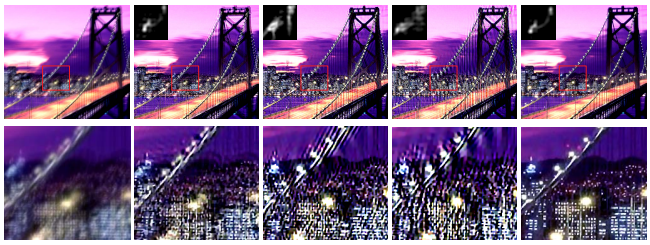

(a) Blurred (b) L_2 (c) L_1 (d) Lorentzian (e) Ours

Figure 7. Effectiveness of the proposed data fidelity term. Deblurring methods based on the conventional data fidelity terms are less effective to generate clear images.

delity terms used in blind image deblurring. Figure 6 shows the quantitative evaluation of the proposed method against those commonly used data fidelity terms on the proposed dataset with saturated pixels (see Section 6 for details). The results in Figure 6 show that the blind image deblurring methods using these conventional data fidelity terms are less effective, as these data fidelity terms are sensitive to outliers as discussed in Section 2.1. Furthermore, the proposed algorithm generates results with higher PSNR values. Figure 7 shows visual comparisons. The deblurred results generated by those commonly used data fidelity terms contain significant ringing artifacts and blur residues. In contrast, our method generates clearer results with fine textures.

Note that although a truncated ℓ_2-norm has the similar shape to $\mathcal{R}(z)$, the truncated ℓ_2-norm based data fidelity term is different from the proposed data fidelity term. Our data fidelity term is continuously differentiable, and its weight in the IRLS method is able to detect the regions of outliers (see Section 4.1 and Figure 5). However, the truncated ℓ_2-norm based data fidelity term is not differentiable and does not have these properties (see the supplemental material for more details).

4.2. Relation with Outlier Handling Methods

Difference from Pan *et al.* [22]. Recently, Pan *et al.* [22] develop an outlier handling method for blind image deblurring. Our method is different from [22] in the following aspects. First, the method [22] uses the conventional ℓ_1-norm based data fidelity term in the intermediate latent image update process, which is less effective for saturated or clipped pixels. Second, this method needs to extract salient edges from the intermediate latent image by an ad-hoc method, which introduces an extra step to detect outliers and then refine the selected edges. However, this strategy is less effective when the salient edges are not correctly selected or the outliers are not detected. Furthermore, the intermediate latent image generated by the method with ℓ_1-norm based data fidelity term usually contains significant artifacts and blur residue, which are likely to be selected in the edge selection step, thus affecting kernel estimation (Figure 7(c)). Third, although Pan *et al.* [22] use a similar robust function in the non-blind deconvolution as the methods [29] do, they do not analyze the property of this function and demonstrate its effectiveness on kernel estimation.

In contrast, the proposed method does not involve the ad-hoc edge selection or extra outlier detection in blur kernel estimation. Instead of finding a good mask to remove outliers, the proposed algorithm estimates intermediate latent images and blur kernels iteratively within a unified MAP framework. With the help of the proposed data fidelity term, the outliers have less effect on blur kernel estimation and latent image estimation as discussed in Section 4.1, thereby facilitating the following kernel estimation.

Figure 5 shows one example where the method [22] does not perform well. The main reason is that the salient edges are not correctly selected (Figure 5(d)-(f)). In contrast, the proposed method generates a clear image with fine details (Figure 5(c)) and the weights derived from the IRLS iteration are able to detect outliers (Figure 5(m)-(o)).

Difference from Cho *et al.* [4] and Whyte *et al.* [29]. As discussed in the introduction, the methods [4, 29] mainly focus on the non-blind deconvolution. To handle blind image deblurring, the methods [4, 29] first manually select some regions without outliers from the input images to estimate blur kernels using the kernel estimation method [3], and then apply their proposed non-blind deconvolution methods. However, it is difficult to select a good image patch when the outliers are ubiquitously distributed in a blurred image (*e.g.*, saturated pixels in Figure 8(a)). Without good kernel estimates, clear images cannot be recovered well. Figure 8 shows an example where the methods [4, 29] do not recover clear images as [3] is less effective for images with outliers.

We note that the methods [4, 29] can be straightforwardly extended to blind deblurring based on the MAP framework, where the intermediate latent image estimation derives from their proposed non-blind deconvolution methods [4, 29] and the kernel estimation is based on the ℓ_1-norm. However, these straightforward extensions do not perform well as shown in Figure 8(c) and (e).

5. Extension to Non-Uniform Deblurring

The proposed method can be directly extended for non-uniform deblurring where the blurred images are acquired from tilting and rotating cameras [6, 7, 25, 28, 30]. Based on the geometric model of camera motion [28, 30], the non-uniform blur model can be expressed as:

$$\mathbf{y} = \mathbf{K}\mathbf{x} + \mathbf{n} = \mathbf{A}\mathbf{k} + \mathbf{n}, \tag{11}$$

where $\mathbf{y}, \mathbf{x}, \mathbf{k}$ and $\mathbf{n}$ are vector forms of y, x, k and n, respectively. In model (11), $\mathbf{K}$ and $\mathbf{A}$ denote the blur kernel matrix and image matrix with respect to the blur kernel $\mathbf{k}$ and latent image $\mathbf{x}$. Based on (11), the non-uniform deblurring process is achieved by alternatively minimizing:

$$\min_{\mathbf{x}} \mathcal{R}(\mathbf{K}\mathbf{x} - \mathbf{y}) + \lambda \|\nabla \mathbf{x}\|_{0.8} \tag{12}$$

(a) Blurred image (b) [3]+[4] (c) Extension of [4] (d) [3]+[29] (e) Extension of [29] (f) Ours

Figure 8. Comparison with Cho *et al*. [4] and Whyte *et al*. [29] and their possible extensions.

and

$$\min_{\mathbf{k}} \mathcal{R}(\mathbf{A}\mathbf{k} - \mathbf{y}) + \gamma \|\mathbf{k}\|_1. \tag{13}$$

We employ the fast forward approximation [7, 21, 33] to estimate the latent image $\mathbf{x}$ and the blur kernel $\mathbf{k}$. The algorithmic details are presented in the supplementary material.

6. Experimental Results

We present experimental evaluations of the proposed algorithm against the state-of-the-art blind deblurring methods. First, we examine our algorithm on two synthetic image datasets with different significant outliers (*i.e*., saturated pixels and impulse noise). Then, we evaluate our method on real captured images with outliers. Finally, we quantitatively evaluate our method on two publicly available image datasets [16, 26] without outliers. As shown in [4, 22, 27], the effects of nonlinear camera response function can be minimized by using raw camera output or alleviated by applying an inverse response curve obtained from camera calibration before kernel estimation. Thus we do not consider the nonlinear camera response function [27] in the following experiments. Due to the comprehensive experiments performed, we only show the main results in this section, and present more results in the supplemental material.

Parameter settings. In all experiments, we set γ and λ in (3) as 0.1 and 0.008, respectively. The parameters a and b in (2) are set to be $459/\sqrt{2\pi}$ and $2601/2$. We empirically set $t_{\max} = 4$ as a trade-off between accuracy and speed. The proposed algorithm is implemented in MATLAB on a computer with an Intel Core i7-4790K CPU and 32 GB RAM. All the color images are converted to grayscale ones in the kernel estimation process. In the final deconvolution process, each color channel is processed independently. The MATLAB code is publicly available on the authors' websites.

Dataset with saturated pixels. To evaluate the effectiveness of the proposed method, we create a dataset containing 5 ground-truth low-light images with saturated pixels (see the supplemental material for details) and 8 kernels from [16]. Similar to [22], each ground-truth image is synthetically blurred by 8 blur kernels and high-intensity pixels are clipped. We also add 1% random noise on each blurred image. For fair comparisons, we use the original implementations of the state-of-the-art methods [3, 8, 20, 22, 23, 33] to estimate blur kernels. The non-blind deconvolution method [4] is used to generate the final deblurring results. We use the PSNR and error ratio [16] as the quality metrics. Figure 9 shows that the proposed algorithm achieves favorable results against the state-of-the-art methods. As the methods [3, 20, 33] are not designed for images with saturated pixels, the PSNR values of the restored images are lower than other methods. Although the method [8] is able to deal with images with saturated areas, it is less effective when the light streaks are not available. Although the dark channel prior based method [23] is able to handle images with saturated pixels, this method is sensitive to image noise. The outlier handling method [22] is based on a heuristic edge selection step for blur kernel estimation. However, it is less effective when the positions of outliers are not detected. In contrast, our method generates images with higher PSNR values. Table 1 reports the average error ratio of the results in Figure 9 and shows that the proposed algorithm performs favorably against the state-of-the-art methods. Figure 10 shows an example where the state-of-the-art methods do not generate clear images. However, our method generates a clear image with fine textures.

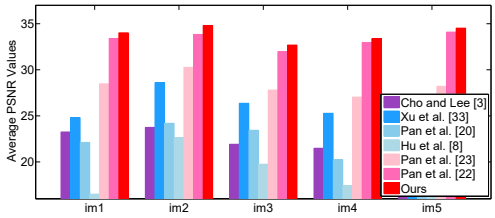

Figure 9. Quantitative evaluation on the dataset with saturated pixels in terms of PSNR.

Dataset with impulse noise. To further evaluate the proposed method, we create a dataset containing 30 ground-truth natural images (see the supplemental material for details) and 8 kernels from [16], in which we add the impulse noise (as it is one of the most common non-Gaussian noise) to each image. The noise density is set to be 0.02. Thus, we have 240 blurred images in total. We evaluate the proposed algorithm against several state-of-the-art deblurring methods including the outlier handling method [22]. We follow the protocol used in the dataset with saturated pixels for fair comparisons. Table 2 reports the average PSNR values of the restored results, where our method achieves a higher P-

Table 1. Quantitative comparison using the dataset with saturated pixels in terms of error ratio metric.

	[3]	[33]	[20]	[8]	[23]	[22]	Ours
Average Error Ratio	18.04	7.42	13.41	34.37	3.83	3.22	**3.09**

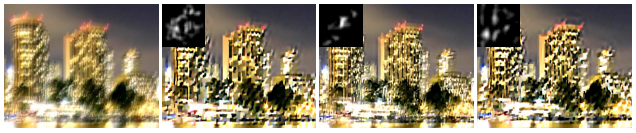

(a) Input PSNR: 14.72 (b) [3] PSNR: 21.60 (c) [33] PSNR: 17.89 (d) [8] PSNR: 20.11

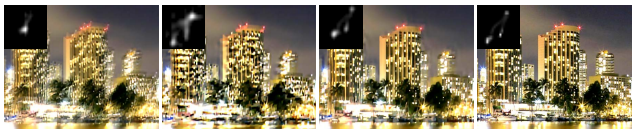

(e) [23] PSNR: 19.33 (f) [22] PSNR: 21.11 (g) Ours PSNR: **23.52** (h) GT

Figure 10. A synthetic example with saturated pixels (Best viewed on high-resolution displays with zoom-in).

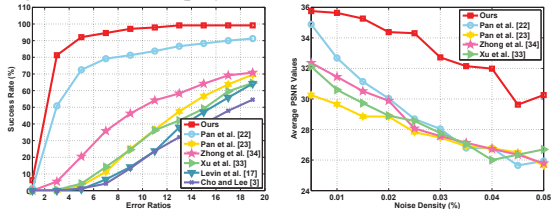

(a) Dataset with impulse noise (b) Robustness to impulse noise

Figure 11. Quantitative evaluations on dataset with impulse noise.

SNR than the others. The error ratio [16] is also used as the quality metric. As Figure 11(a) shows, our method performs favorably against the state-of-the-art methods.

We evaluate our method using images with different noise densities. Figure 11(b) shows that the proposed algorithm performs well even when the noise density is high.

Figure 12 shows a synthetic example with impulse noise from the dataset. Since the conventional data fidelity terms are not robust to outliers, the state-of-the-art blind deblurring algorithms [3, 17, 33] do not estimate the blur kernels well, thus resulting in blurred results with significant ringing artifacts (Figure 12(b), (c), and (d)). The method [34] is designed to deal with Gaussian noise, but less effective for impulse noise. Although the recent method [23] is able to address saturated images, it is less effective for images with noise as pointed in the work. Thus, the blur kernels estimated by [23, 34] are not accurate which accordingly leads to results with significant ringing artifacts (Figure 12(e) and (f)). The method [22] is designed to handle outliers including impulse noise. However, this method involves a heuristic edge selection and outlier detection step and is less effective when the edges are not correctly selected or the outliers are not detected (Figure 12(g)). In contrast, our estimated blur kernel is visually close to the ground-truth blur kernel, and the recovered latent image contains clearer details and fewer ringing artifacts (Figure 12(h)).

Real images. We evaluate the proposed algorithm and other methods using real images with outliers. Figures 13

(a) Input PSNR: 16.00 (b) [3] PSNR: 20.05 (c) [17] PSNR: 26.13 (d) [33] PSNR: 26.12

(e) [34] PSNR: 22.31 (f) [22] PSNR: 28.76 (g) Ours PSNR: **31.37** (h) GT

Figure 12. A synthetic example with impulse noise (Best viewed on high-resolution displays with zoom-in).

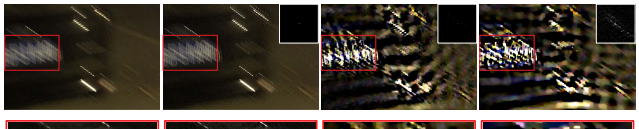

(a) Blurred (b) [3] (c) [17] (d) [33]

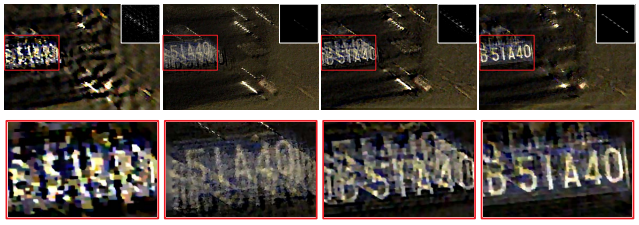

(e) [8] (f) [23] (g) [22] (h) Ours

Figure 13. A real captured image with numerous saturated pixels.

and 14 show two challenging real captured images with numerous saturated areas and unknown noise. The state-of-the-art methods [3, 17, 23, 33] do not perform well on these examples due to the effects of saturated areas. The method by Hu *et al*. [8] does not generate clear results either due to unavailable light streaks (Figures 13(e) and 14(e)). The deblurred results of [22] contain ringing artifacts, and some details are not recovered well. In contrast, our method successfully estimates the blur kernels and generates better-deblurred results. Furthermore, the comparison results shown in Figures 13 and 14 demonstrate that the proposed algorithm is able to prevent the effects of outliers in blur kernel estimation.

Non-uniform examples. As our method can be extended to

Table 2. Quantitative comparison on the proposed dataset with impulse noise in terms of PSNR.

	[3]	[17]	[33]	[34]	[23]	[22]	Ours
Average PSNR	28.5819	27.1834	30.6736	28.5304	29.3544	32.0176	**34.5818**

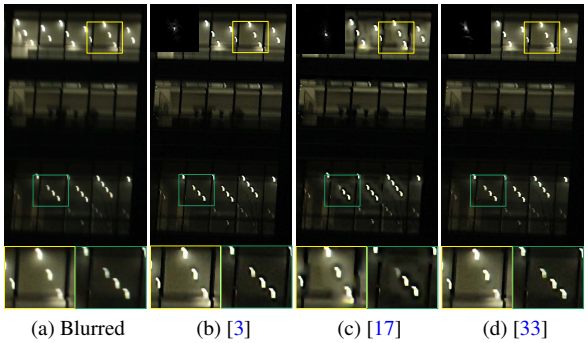

(a) Blurred (b) [3] (c) [17] (d) [33]

(e) [8] (f) [23] (g) [22] (h) Ours

Figure 14. A real example with numerous saturated pixels.

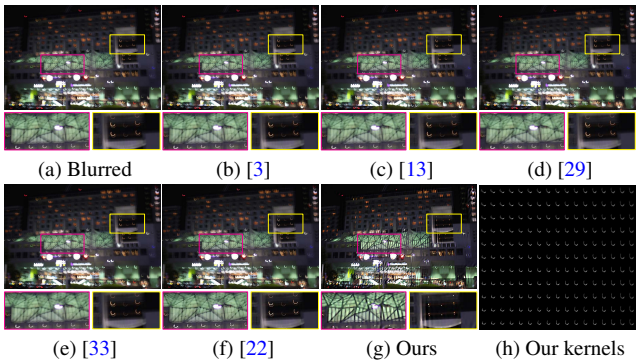

(a) Blurred (b) [3] (c) [13] (d) [29]

(e) [33] (f) [22] (g) Ours (h) Our kernels

Figure 15. The proposed algorithm applies to images with non-uniform blur and generates results with fewer ringing artifacts (Best viewed on high-resolution displays with zoom-in).

deal with non-uniform blur, we also report results on an image degraded by spatially-variant motion blur in Figure 15. Due to saturated pixels, the state-of-the-art non-uniform deblurring methods [13, 29] do not perform well. Compared to the outlier handling method [22], our method generates an image with fewer artifacts and clearer textures.

Benchmark datasets without outliers. Our method can be applied to deblur natural images without outliers. To verify the effectiveness of the proposed method, we use the natural image benchmark datasets [16, 26] for quantitative evaluations and follow the protocols of [16, 26] for fair comparisons. Although the proposed algorithm focuses on handling outliers, our method achieves comparable results a-

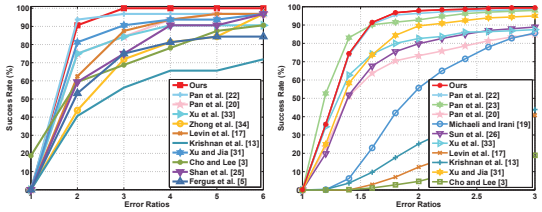

(a) Results on the dataset [16] (b) Results on the dataset [26]

Figure 16. Quantitative evaluations on two benchmark datasets.

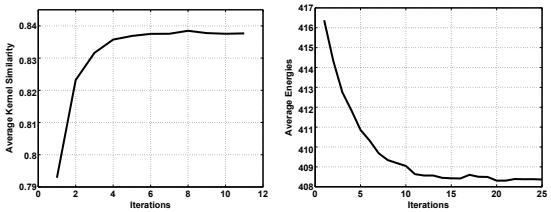

Figure 17. Convergence property of the proposed algorithm.

gainst the state-of-the-art methods [3, 5, 13, 17, 19, 20, 22, 23, 25, 26, 31, 33, 34] on both datasets without outliers, as shown in Figure 16. More experimental results are included in the supplemental material.

6.1. Convergence of Proposed Algorithm

As our energy function is nonlinear and highly nonconvex, a natural question is whether our optimization method converges (*e.g.*, to a good local minimum) or not. We quantitatively evaluate the convergence property of the proposed algorithm on the proposed dataset with impulse noise (see Section 6 for details). The results shown in Figure 17 demonstrate that the proposed method converges after less than 12 iterations, in terms of the average kernel similarity values and the energies computed from (3).

7. Conclusions

In this paper, we propose a robust method to measure the goodness-of-fit to minimize the effects of outliers in the blur kernel estimation. We analyze how the proposed algorithm handles outliers, discuss the relationship between the proposed method and other related methods, and show that the proposed algorithm generates reliable intermediate latent images for kernel estimation without ad-hoc detection process. Extensive experimental evaluations on benchmark datasets and real images demonstrate the proposed method performs favorably against the state-of-the-art methods for uniform and non-uniform deblurring.

Acknowledgements: This work is supported in part by NSFC (No. 61572099 and 61522203), NSF CAREER (No. 1149783), 973 Program (No. 2014CB347600), NSF of Jiangsu Province (No. BK20140058), the National Key R&D Program of China (No. 2016YFB1001001), and gifts from Adobe and Nvidia.

References

[1] J.-F. Cai, H. Ji, C. Liu, and Z. Shen. Blind motion deblurring from a single image using sparse approximation. In *CVPR*, pages 104–111, 2009.

[2] J. Chen, L. Yuan, C. Tang, and L. Quan. Robust dual motion deblurring. In *CVPR*, 2008.

[3] S. Cho and S. Lee. Fast motion deblurring. *ACM TOG*, 28(5):145, 2009.

[4] S. Cho, J. Wang, and S. Lee. Handling outliers in non-blind image deconvolution. In *ICCV*, pages 495–502, 2011.

[5] R. Fergus, B. Singh, A. Hertzmann, S. T. Roweis, and W. T. Freeman. Removing camera shake from a single photograph. *ACM TOG*, 25(3):787–794, 2006.

[6] A. Gupta, N. Joshi, C. L. Zitnick, M. Cohen, and B. Curless. Single image deblurring using motion density functions. In *ECCV*, pages 171–184, 2010.

[7] M. Hirsch, C. J. Schuler, S. Harmeling, and B. Schölkopf. Fast removal of non-uniform camera shake. In *ICCV*, pages 463–470, 2011.

[8] Z. Hu, S. Cho, J. Wang, and M. H. Yang. Deblurring low-light images with light streaks. In *CVPR*, pages 3382–3389, 2014.

[9] P. J. Huber. *Robust Statistics*. Springer, 1981.

[10] J. Jia. *Mathematical models and practical solvers for uniform motion deblurring*. Cambridge University Press, 2014.

[11] N. Joshi, R. Szeliski, and D. J. Kriegman. PSF estimation using sharp edge prediction. In *CVPR*, pages 1–8, 2008.

[12] R. Köhler, M. Hirsch, B. Mohler, B. Schölkopf, and S. Harmeling. Recording and playback of camera shake: Benchmarking blind deconvolution with a real-world database. In *ECCV*, pages 27–40, 2012.

[13] D. Krishnan, T. Tay, and R. Fergus. Blind deconvolution using a normalized sparsity measure. In *CVPR*, pages 2657–2664, 2011.

[14] S. Lee and S. Cho. Recent advances in image deblurring. In *SIGGRAPH Asia 2013 Courses*, 2013.

[15] A. Levin, R. Fergus, F. Durand, and W. T. Freeman. Image and depth from a conventional camera with a coded aperture. *ACM TOG*, 26(3):70, 2007.

[16] A. Levin, Y. Weiss, F. Durand, and W. T. Freeman. Understanding and evaluating blind deconvolution algorithms. In *CVPR*, pages 1964–1971, 2009.

[17] A. Levin, Y. Weiss, F. Durand, and W. T. Freeman. Efficient marginal likelihood optimization in blind deconvolution. In *CVPR*, pages 2657–2664, 2011.

[18] H. Liu, X. Sun, L. Fang, and F. Wu. Deblurring saturated night image with function-form kernel. *IEEE TIP*, 24(11):4637–4650, 2015.

[19] T. Michaeli and M. Irani. Blind deblurring using internal patch recurrence. In *ECCV*, pages 783–798, 2014.

[20] J. Pan, Z. Hu, Z. Su, and M.-H. Yang. Deblurring text images via L_0-regularized intensity and gradient prior. In *CVPR*, pages 2901–2908, 2014.

[21] J. Pan, Z. Hu, Z. Su, and M.-H. Yang. L_0-regularized intensity and gradient prior for deblurring text images and beyond. *IEEE TPAMI*, 39(2):342–355, 2017.

[22] J. Pan, Z. Lin, Z. Su, and M.-H. Yang. Robust kernel estimation with outliers handling for image deblurring. In *CVPR*, pages 2800–2808, 2016.

[23] J. Pan, D. Sun, H. Pfister, and M.-H. Yang. Blind image deblurring using dark channel prior. In *CVPR*, pages 1628–1636, 2016.

[24] D. Perrone and P. Favaro. Total variation blind deconvolution: The devil is in the details. In *CVPR*, pages 2909–2916, 2014.

[25] Q. Shan, J. Jia, and A. Agarwala. High-quality motion deblurring from a single image. *ACM TOG*, 27(3):73, 2008.

[26] L. Sun, S. Cho, J. Wang, and J. Hays. Edge-based blur kernel estimation using patch priors. In *ICCP*, 2013.

[27] Y.-W. Tai, X. Chen, S. Kim, S. J. Kim, F. Li, J. Yang, J. Yu, Y. Matsushita, and M. S. Brown. Nonlinear camera response functions and image deblurring: Theoretical analysis and practice. *IEEE TPAMI*, 35(10):2498–2512, 2013.

[28] Y.-W. Tai, P. Tan, and M. S. Brown. Richardson-lucy deblurring for scenes under a projective motion path. *IEEE TPAMI*, 33(8):1603–1618, 2011.

[29] O. Whyte, J. Sivic, and A. Zisserman. Deblurring shaken and partially saturated images. *IJCV*, 110(2):185–201, 2014.

[30] O. Whyte, J. Sivic, A. Zisserman, and J. Ponce. Non-uniform deblurring for shaken images. *IJCV*, 98(2):168–186, 2012.

[31] L. Xu and J. Jia. Two-phase kernel estimation for robust motion deblurring. In *ECCV*, pages 157–170, 2010.

[32] L. Xu, C. Lu, Y. Xu, and J. Jia. Image smoothing via L_0 gradient minimization. *ACM TOG*, 30(6):174, 2011.

[33] L. Xu, S. Zheng, and J. Jia. Unnatural L_0 sparse representation for natural image deblurring. In *CVPR*, pages 1107–1114, 2013.

[34] L. Zhong, S. Cho, D. Metaxas, S. Paris, and J. Wang. Handling noise in single image deblurring using directional filters. In *CVPR*, pages 612–619, 2013.